PROCESSES AFFECTING THE CR CHONDRITES PARENT BODY: PETROLOGY, MINERALOGY AND CHEMICAL COMPOSITION OF THE MATRICES OF ANTARCTIC CR CARBONACEOUS CHONDRITES. N. M. Abreu[1], [1]Earth Science Program, Penn State DuBois abreu@psu.edu.

Introduction: Scales devised to quantify the degree of aqueous alteration of CR chondrites have generated contradictory classifications [1,2]. CRs record a broad range of asteroidal alteration features [e.g., 1-6]. Most CRs are classified as type 2. The least altered CRs have been argued to be to petrologic type 3 [5], whereas the CRs that record most extensive signs of aqueous alteration are type 1 [6]. Fine-grained mineralogical and compositional studies of the matrices of 10 Antarctic CRs were collected via FEG-SEM, FEG-EPMA, and TEM. Samples names are abbreviated as follows: EET 96259, EET96; GRA 95229, GRA95; GRA 06100, GRA06; GRO 95577, GRO95; GRO 03116, GRO 03; LAP 02432, LAP02; LAP 04516, LAP045; LAP 04720, LAP047; MIL 07525, MIL07; and MIL 090001, MIL09. Observations are compared the aqueous alteration scales.

Results: Less than half of chondrules in the CRs show signs of mesostasis replacement by chlorite or serpentine. Matrix is texturally heterogeneous, containing abundant chondrule fragments and small clasts that are enriched in elongated, feathery sulfides and framboidal and platelet magnetite grains. Opaques in some clasts are oriented. Chemical composition of 8 CRs was determined using via EPMA, using 10μm beam (Table 1). Large intra- and inter-chondrite variations are observed in all elements. Through an ongoing study of CRs, 24 FIB sections were extracted from representative fine-grained regions from 10 CRs. Observed mineral assemblages are given in Table 2. Owing to marked differences in mineralogy the details of the mineralogy of GRA06 matrix are discussed elsewhere [7]. CR matrices are dominated by amorphous Fe-Mg-silicates. Neither increased phyllosilicates abundance near chondrules nor phyllosilicates layers around chondrules have been observed. Phyllosilicate abundance increases with aqueous alteration. However, no correlation between the textural characteristics of matrix and phyllosilicates abundance has been observed; more extensively altered chondrites contain more phyllosilicates in all fine-grained regions.

Discussion: The following sub-μm secondary phases are used to determine the degree of aqueous alteration: (1) ratio of Fe-Mg amorphous silicates to phyllosilicates, (2) size of phyllosilicates, (3) abundance of magnetite, (4) replacement of Fe-Ni sulfides (partial oxidation to replacement by tochilinite). The sequence from the least to the most altered CRs is: GRA95, LAP02, EET96, MIL09, MIL07, LAP047, LAP045, GRO95. GRA06 and GRO03 are excluded due to significant differences in the matrix mineralogy, which have been attributed to the heating [7].

Sub-μm observations are not in agreement with proposed compositional indicators of aqueous alteration (Figs. 1-2) or with alteration scales. [8] suggested that increasing degrees of aqueous alteration resulted in higher Mg concentration relative to Fe in matrix, owing to replacement of Mg-phenocrysts by phyllosilicates. There is no correlation between aqueous alteration and Mg matrix concentration (Fig. 1). As CR aqueous alteration proceeds, Fe is also mobilized into to the matrix via oxidation and hydration of Fe-Ni metal, which are abundant in CR chondrites. Thus the correlation between Mg and aqueous alteration is weak. Decreasing and heterogeneous distribution of S have been suggested to accompany aqueous alteration, owing to coarsening of nanophase Fe-sulfides [2,8]. However, Fig. 1 shows that there is no simple correlation between matrix sulfide content and aqueous alteration. This could be explained by incipient formation of nanophase tochilinite observed in some extensively altered CRs (e.g., LAP047, LAP045, MIL07) that do not contain large amounts of micron-sized sulfides.

Table 1. Average composition of matrices of CRs. b.d.: below detection; n.m. – not measured.

Matrix	EET96	GRA95	GRA06	GRO03	LAP045	LAP047	MIL07	MIL09
Al_2O_3	2.0	2.0	2.1	1.4	1.7	1.7	2.1	3.7
CaO	1.2	1.0	1.5	1.1	1.1	2.5	2.0	0.9
TiO_2	b.d.	0.1	0.1	0.1	0.1	b.d.	0.1	0.1
MgO	17.1	14.9	14.8	12.9	14.6	17.2	15.8	10.4
SiO_2	30.6	30.1	27.3	23.0	27.1	27.7	29.0	28.2
Cr_2O_3	0.4	0.2	0.3	0.4	0.4	0.4	0.4	0.3
MnO	0.2	0.3	0.3	0.2	n.m.	0.3	0.3	0.2
P_2O_5	0.3	0.2	0.2	0.2	n.m.	0.2	0.4	0.2
Na_2O	0.3	0.9	0.4	0.3	0.4	1.4	0.3	0.3
K_2O	0.1	0.1	0.1	0.1	b.d.	0.1	b.d.	0.1
NiO	1.5	1.3	2.0	1.8	1.8	2.2	2.1	3.4
FeO	30.3	29.2	36.8	46.5	29.7	32.6	30.1	36.6
S	2.8	2.2	0.6	1.9	3.6	0.5	3.0	1.4
Total	86.8	82.6	86.5	89.8	80.4	86.7	85.6	85.6

Clusters of meteorites (around petrologic type 2.5-2.6 in [1] and around petrologic type 2.8 in [2]) have widely divergent secondary mineralogies. Based on bulk water/OH and phyllosilicate abundances measured by [1], the sequence is: LAP047(2.6); GRA95(2.5); LAP02(2.5); GRO95(1.3). Differences between this classification scheme and the petrologic record were explained by heterogeneities in (more altered) dark inclusion abundance and by differences in

the temperature of aqueous alteration [1]. Another possibility is that since unaltered amorphous silicates may be hydrated [9], wt.% H may not be a direct proxy asteroidal aqueous alteration.

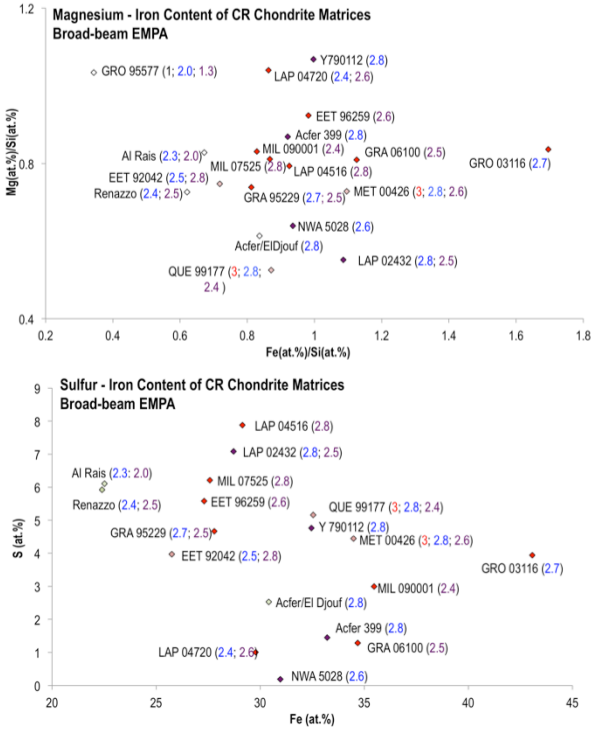

Fig. 1. Average Mg/Si v. Fe/Si and Fe v. S. Petrologic sub-types from [5]-red; [2]-blue; [1]-purple.

Table 2. Sub-µm CR matrix mineralogy (TEM/EDS).

Meteorite	Common Matrix Minerals	Scarce Minerals
EET 96259	Fe-Mg amorph silicate, Ferrolizardite, Fe-oxide (prob. Wustite)	Fe-sulfide
GRA 95229	Fe-Mg amorph silicate, Ferrolizardite, FeNi-sulfide	Forsteritic Olivine, Enstatite, Fe-oxide, C-nanoglobules
GRA 06100	Fe-Mg amorph silicate, Fe-rich Serpentine, FeNi-sulfide, FeNi metal, Fe-silicide, Fe-oxide (prob. Wustite and Magnetite), Hisingerite	Forsterite, Fayalite, Enstatite, Garnet
GRO 95577	Fe-Mg amorph silicate, Fe-rich Serpentine, FeNi-sulfide	
GRO 03116	Fe-Mg amorph silicate, Fe-rich Serpentine, FeNi-sulfide, FeNi metal	Forsterite, Ferrosilite
LAP 02432	Fe-Mg amorph silicate, Fe-rich Serpentine, FeNi-sulfide	Fe-oxide (prob. Wustite,Magnetite),
LAP 04516	Fe-Mg amorph silicate, Fe-rich Serpentine, Tochilinite, FeNi-sulfide	Diopside, Pigeonite
LAP 04720	Fe-Mg amorph silicate, Fe-rich Serpentine, FeNi-sulfide	Forsterite, Fayalite, Enstatite, Fe-silicide
MIL 07525	Fe-Mg amorph silicate, Fe-rich Serpentine, FeNi-sulfide	Tochilinite
MIL 090001	Fe-Mg amorph silicate, Fe-rich Serpentine, FeNi-sulfide	

Based on petrologic and O-isotopic indicators, [2] obtained the sequence: LAP02 (2.8); MIL07 (2.8); LAP045 (2.8); GRA95 (2.7); EET96 (2.4); LAP047 (2.4); GRO95 (2.0). TEM observations suggest that [2] overestimated the presence of phyllosilicates in weakly altered CRs based on BSE and low total EMPA. This may explain the cluster of weakly and moderately altered CRs around petrologic sub-type 2.8. Smooth rims described in LAP02 are assumed to be rich in phyllosilicates [10]. A FIB section extracted from such rim (Fig. 2) does not contain phyllosilicates.

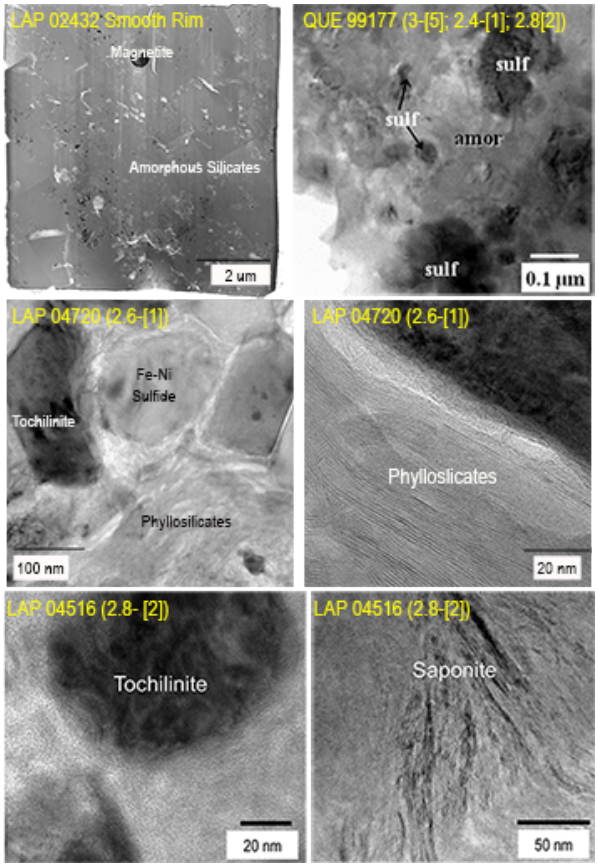

Fig. 2. TEM images of (a) smooth rim in LAP 02432; (b) representative mineralogical assemblages of CR.

Conclusions: Aqueous alteration scales for the CRs need to be consistent with mineralogical changes recorded by matrices. Bulk compositional and >µm petrologic indicators of aqueous alteration are not good predictors for the abundance of secondary matrix phases and thus cannot substitute sub-µm observations.

References: [1] Alexander et al. (2013) *GCA* 123, 244–260. [2] Harju et al. (2014) *GCA* 139, 267–292. [3] Zolensky et al. (1993) *GCA* 57, 3123-3148. [4] Weisberg et al. (1993) *GCA* 57, 1567. [5] Abreu & Brearley (2010) *GCA* 74, 1146-1171. [6] Weisberg & Huber (2007) *MAPS*, 42, 1495-1503. [7] Abreu et al. (2014) *LPS XLV,* Abstract # 2753. [8] Abreu (2007) Ph.D. Dissertation. [9] Le Guillou & Brearley (2014). *GCA,* 131, 344-367. [10] Rubin & Wasson (2009) *GCA,* 73, 1436-1460.

Funded by NNX11AH10G to NMA.